Evaluation of A-site cation-deficient $(Ba_{0.5}Sr_{0.5})_{1−x}Co_{0.8}Fe_{0.2}O_{3−δ}$ $(x > 0)$ perovskite as a solid-oxide fuel cell cathode

Wei Zhou, Ran Ran, Zongping Shao*, Wanqin Jin, Nanping Xu

State Key Laboratory of Materials-Oriented Chemical Engineering, College of Chemistry and Chemical Engineering, Nanjing University of Technology, No. 5 Xin Mofan Road, Nanjing 210009, PR China

ABSTRACT

A-site cation-deficient $(Ba_{0.5}Sr_{0.5})_{1−x}Co_{0.8}Fe_{0.2}O_{3−δ}$ $((BS)_{1−x}CF)$ oxides were synthesized and evaluated as cathode materials for intermediate-temperature solid-oxide fuel cells (ITSOFCs). The material's thermal expansion coefficient, electrical conductivity, oxygen desorption property, and electrocatalytic activity were measured. A decrease in both the electronic conductivity and the thermal expansion coefficient was observed for increasing values of the stoichiometric coefficient, x. This effect was attributed to the creation of additional oxygen vacancies, the suppression of variation in the oxidation states of cobalt and iron, and the suppression of the spin-state transitions of cobalt ions. The increase in A-site cation deficiency resulted in a steady increase in cathode polarization resistance, because impurities formed at the cathode/electrolyte interface, reducing the electronic conductivity. A single SOFC equipped with a $BS_{0.97}CF$ cathode exhibited peak power densities of 694 and 893 mW cm^{-2} at 600 and 650 °C, respectively, and these results were comparable with those obtained with a $Ba_{0.5}Sr_{0.5}Co_{0.8}Fe_{0.2}O_{3−δ}$ cathode. Slightly A-site cation-deficient $(BS)_{1−x}CF$ oxides were still highly promising cathodes for reduced temperature SOFCs.

© 2008 Elsevier B.V. All rights reserved.

1. Introduction

Solid-oxide fuel cells (SOFCs) are electrochemical power generation devices characterized by high-energy conversion efficiency, low emission, and excellent fuel flexibility. Typical SOFCs operate at ∼1000 °C, and elevated temperatures introduce a series of problems such as the sintering of electrodes, high reactivity between cell components, and strict requirements on interconnected materials. Consequently, there is increasing interest in intermediate-temperature (IT)-SOFCs, which are operated in the range of 500–800 °C [1–5]. The decrease in operating temperature, however, increases the cells' overpotential, and the main contributor to this increase is the cathode [6,7]. The development of new cathode materials with low polarization resistance is therefore of great importance to achieving high power densities at reduced temperatures.

$SrCoO_{3−δ}$-based, mixed ionic and electronic conducting materials, such as $La_{1−x}Sr_xCo_{1−y}Fe_yO_{3−δ}$ [8–11], $Sm_{1−x}Sr_xCoO_{3−δ}$ [12–15], and $Ba_{1−x}Sr_xCo_{1−y}Fe_yO_{3−δ}$ [16–20], are promising candidates for cathode material for use in reduced temperature SOFCs. In the $Ba_{1−x}Sr_xCo_{1−y}Fe_yO_{3−δ}$ family, $Ba_{0.5}Sr_{0.5}Co_{0.8}Fe_{0.2}O_{3−δ}$ (BSCF) exhibits the highest electrocatalytic activity for oxygen reduction because of its high oxygen surface-exchange kinetics and high oxygen bulk diffusion rate at intermediate temperatures [21]. On the other hand, some studies have demonstrated that introducing A-site cation deficiencies into the lattice structure of perovskite oxides significantly alters the material's physical and chemical properties [22–26]. For example, Kostogloudis and Ftikos observed that the A-site cation-deficient compound, $(La_{0.6}Sr_{0.4})_{1−x}Co_{0.2}Fe_{0.8}O_{3−δ}$, had both a lower thermal expansion coefficient (TEC) and a lower electronic conductivity than the corresponding cation-stoichiometric material ($La_{0.6}Sr_{0.4}Co_{0.2}Fe_{0.8}O_{3−δ}$) [22]. Mineshige et al. suggested that the reduced electronic conductivity could be attributed to the creation of additional oxygen vacancies [23]. Very recently, it was confirmed that additional oxygen vacancies are indeed beneficial to the oxygen reduction reaction [24]. The superior performance of A-site cation-deficient LSCF cathodes was also reported by Doshi et al., who found that the initial cathode resistance was as low as 0.1 Ω cm^2 at 500 °C [25].

In our recent investigation of mixed oxygen-conducting membranes, we observed that introducing the proper amount of A-site cation deficiency into BSCF (i.e., the formation of a $(Ba_{0.5}Sr_{0.5})_{1−x}Co_{0.8}Fe_{0.2}O_{3−δ}$ $((BS)_{1−x}CF)$ oxide) significantly improved the membrane's oxygen permeability [27]. It was also demonstrated that creating additional oxygen vacancies from the

* Corresponding author. Tel.: +86 25 83587722; fax: +86 25 83365813.
E-mail address: shaozp@njut.edu.cn (Z. Shao).

A-site deficiencies facilitated oxygen ion diffusion within the oxide bulk, and that this effect was responsible for the improved oxygen permeability of the related membranes.

In this study, we systematically evaluated the effect of A-site cation deficiency on the performance of $(BS)_{1-x}CF$ ($x = 0.03–0.20$) perovskite cathodes in ITSOFCs fabricated with a samaria-doped ceria electrolyte. The thermal expansion properties, electrical conductivities, electrochemical properties, and phase reactions between the cathode and the electrolyte of these materials were investigated. Taking all these factors into account, an optimal concentration of A-site cation-deficiencies was proposed.

2. Experimental

2.1. Material synthesis and cell fabrication

The $(BS)_{1-x}CF$ oxide powders were synthesized via a standard combined EDTA-citrate complexing sol–gel process. The procedure is described in detail in our previous publications [28,29]. Metal nitrates $Ba(NO_3)_2$, $Sr(NO_3)_2$, $Co(NO_3)_2$, and $Fe(NO_3)_3$ were used as the raw materials. Each metal nitrate was prepared as a separate aqueous solution, and a standard EDTA titration method was used to determine the precise concentrations of these solutions. In accordance with the composition of the $(BS)_{1-x}CF$ material, the required amounts of metal nitrate solutions were mixed, and EDTA and citric acid were added to serve as complexing agents. The pH value of the solution was adjusted to ∼6 with NH_4OH. The molar ratio of total metal ions/EDTA/citric acid was set at 1:1:2. The water was evaporated at 90 °C yielding transparent gels. The gels were pre-fired at 250 °C and then calcined at 1000 °C for 5 h under an air atmosphere, and the resulting products possessed the desired final phase structure.

Symmetrical cells with electrode|SDC|electrode configurations were fabricated for the impedance studies. Dense SDC pellets, which were 12.0 mm in diameter and 0.8 mm thick, were prepared through dry pressing. The pellets were then sintered at 1350 °C for 5 h. The $(BS)_{1-x}CF$ cathode powder was first dispersed in a pre-mixed solution of glycerol, ethylene glycol, and isopropyl alcohol, and a colloidal suspension was formed via high-energy ball milling (Fritsch, Pulverisettle 6) at 400 rpm for 0.5 h. The resulting slurry was painted onto both surfaces of the SDC pellet in symmetric fashion and subsequently calcined at 1000 °C for 2 h under an air atmosphere.

The performance of the $(BS)_{1-x}CF$ cathode was also evaluated in a complete electrochemical cell. Anode-supported thin-film electrolyte dual-layer cells were prepared via dual dry-pressing and subsequent high-temperature sintering [30]. Anode powders consisting of 60 wt% NiO and 40 wt% SDC were prepared through the mechanical mixing of NiO and SDC in an agate mortar. The electrolyte of the green bi-layer pellets was densified through firing at 1450 °C for 5 h under an air atmosphere. The cathode slurry was then painted onto the central surface of the densified electrolyte and fired at 1000 °C for 2 h under an air atmosphere. The resulting coin-shaped cathode was 10–20 μm thick and had an effective area of 0.42 cm^2.

2.2. Basic characterizations

The chemical compatibility between the cathode and the electrolyte materials was assessed. Powders consisting of $(BS)_{1-x}CF$ ($x = 0.03–0.20$) (70 wt%) and SDC (30 wt%) were well mixed and calcined at 1000 °C for 2 h under an air atmosphere. The phase composition of the mixture after firing was analyzed by X-ray diffraction (XRD, Bruker D8 Advance) at room temperature.

The oxygen desorption properties of the materials were studied using an oxygen temperature-programmed desorption (O_2–TPD) technique. About 150 mg of $(BS)_{1-x}CF$ powders were loaded into a quartz tube, which was then placed into a single-zone temperature programmable tube furnace. Argon carrier gas flowed through the tube at a rate of 20 ml min^{-1} (STP: standard temperature and pressure). The temperature was increased from 50 to 950 °C at 10 °C min^{-1}, and the effluent gases were monitored with a mass spectrometer (MS, Hiden, QIC-20).

The calcined powder was palletized in the form of rectangular bars of dimensions of 6 mm × 6 mm × 20 mm under a uniaxial pressure of 200 MPa, and then fired at 1200 °C for 5 h for both the measurements of electrical conductivities and thermal expansion coefficients. All the samples used for the measurements had densities of >93% of the theoretical values. The electrical conductivities were measured via four-terminal DC technique using Ag paste electrodes. The current and voltage were measured using a Keithley 2420 source meter at intervals of 5 °C over a temperature range of 300–900 °C under an air atmosphere. TECs were measured using a Netsch DIL 402C/3/G dilatometer from room temperature to 750 °C with an air-purge flow rate of 50 ml min^{-1}.

2.3. Electrochemical performance test

An electrochemical cell with a four-terminal configuration was constructed, and the *I–V* polarization was measured using a Keithley 2420 source meter. Humidified (3% H_2O) H_2 fuel was fed into the anode chamber at a flow rate of 80 ml min^{-1} (STP), and ambient air served as the oxidant gas. Gas flow rates were controlled with mass flow controllers, and silver paste was used as the current collector.

The electrode performance was investigated via an ac impedance method using an electrochemical workstation composed of a Solartron 1260A frequency response analyzer and a Solartron 1287 potentiostat. The applied frequency range was from 0.01 Hz to 100 kHz, and the signal amplitude was 10 mV under open cell voltage (OCV) conditions. The overall impedance data were fitted using the complex non-linear least squares (CNLS) fitting program from the Z-View 2.9b software.

3. Results and discussion

3.1. Phase structure

The X-ray diffraction patterns of $(BS)_{1-x}CF$ ($x = 0.00–0.30$), acquired at room temperature are presented in Fig. 1. The oxides with $x = 0.0–0.15$ possess a perovskite phase structure with cubic symmetry, while oxides with $x = 0.20$ possess a $(Fe,Co)_3O_4$ impurity phase. This suggests that the A-site cation deficiency fraction (x) was limited to approximately 0.15 for $(BS)_{1-x}CF$. As the A-site cation deficiency increases up to values of $x = 0.20$, the main diffraction peaks of the $(BS)_{1-x}CF$ perovskite gradually shift to higher values of 2θ, which indicates shrinkage of the perovskite lattice. In our previous study, we found that charge-balance of A-site deficient BSCF was compensated by creation of additional oxygen vacancies in BSCF lattice [27]. The increase of oxygen vacancies may promote the electrochemical catalytic activity for oxygen reduction.

3.2. Thermal expansion

TECs of both the electrolyte and electrode layers must be well matched to ensure long-term SOFC operational stability. One distinguishing feature of cobalt-based cathode materials is their high TECs [31]. This property is attributed to crystal expansion from anharmonic atomic vibrations, which depend on the electrostatic
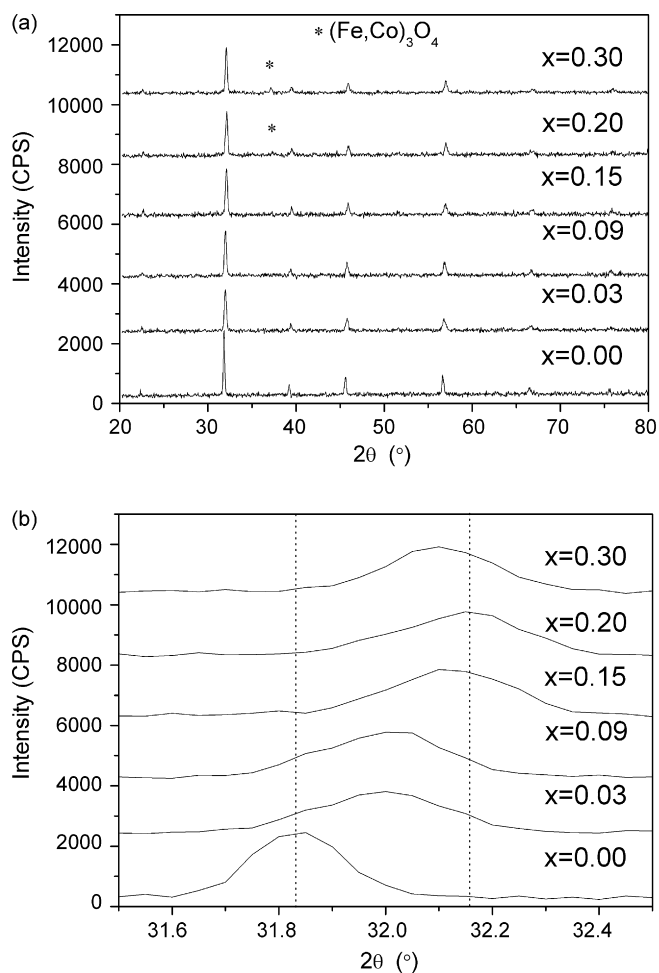
Fig. 1. (a and b) XRD patterns of $(BS)_{1-x}CF$ ($x = 0.00–0.30$) powders calcined at 1000 °C for 5 h under an air atmosphere.

attraction forces within the lattice [31], and to chemical expansion, which is induced by both the cobalt ion spin transition and the thermal/chemical reduction of cobalt ions to lower oxidation states [32].

The thermal expansion curves for the $(BS)_{1-x}CF$ ($x = 0–0.20$) materials are presented in Fig. 2, and the calculated TEC values
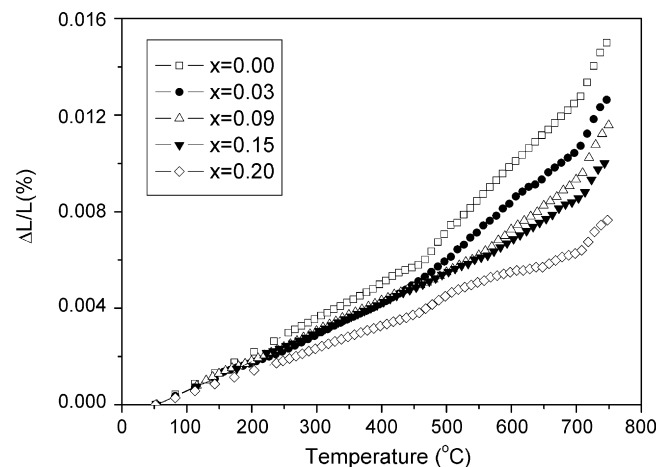
Table 1
Linear TECs (10^{-6} K^{-1}) of $(BS)_{1-x}CF$ ($x = 0.00–0.20$) oxides calculated from the thermal expansion curves between various temperature ranges

x	50–400 °C	450–700 °C	700–750 °C	50–750 °C
0.00	14.4	27.5	58.1	21.4
0.03	11.9	22.7	50.7	18.0
0.09	12.3	18.3	48.8	17.1
0.15	12.1	14.9	36.3	15.3
0.20	9.5	9.3	33.1	10.9

for different temperature ranges are listed in Table 1. The TEC is highly dependent upon both the A-site cation deficiency fraction (x) and the selected temperature range. The TECs decrease with increasing the A-site cation deficiency, especially in the 450–750 °C temperature range. Both Kostogloudis and Ftikos [22] and Hansen and Vels Hansen [24] reported similar trends for $(La_{0.6}Sr_{0.4})_{1-x}Co_{0.2}Fe_{0.8}O_{3-\delta}$ ($x = 0.00–0.15$) oxides. Increased electrostatic attraction resulting from decreases in the lattice parameter may be responsible for this phenomenon.

The TEC of the $(BS)_{1-x}CF$ perovskites is also closely correlated with the chemical expansion effects resulting from changes in the point defect concentration and the spin state of cobalt ions [24]. At elevated temperatures, the release of molecular oxygen, which can be detected *in situ* using a mass spectrometer, follows the thermal reduction of the cobalt and iron ions in $(BS)_{1-x}CF$. Temperature-programmed oxygen desorption curves (O_2–TPD), measured for $(BS)_{1-x}CF$ oxides with varying A-site cation deficiency, are depicted in Fig. 3. Oxygen desorption is observed for two separate onset temperatures, approximately 300 and 800 °C, and for the sake of convenience these desorption processes are labeled α- and β-oxygen [33]. The lower-temperature oxygen desorption process (α-oxygen) is associated with the reduction of Co^{4+} and/or Fe^{4+} to Co^{3+} and/or Fe^{3+}, respectively, and the β-oxygen desorption process is associated with the reduction of Co^{3+} to Co^{2+}. The total amount of desorbed α-oxygen decreases with increasing A-site deficiency, but the total amount of desorbed β-oxygen increases (Table 2). In combination with previous results (Table 1), it is likely that the thermal reduction of Co^{4+}/Fe^{4+} to Co^{3+}/Fe^{3+} within the 400–700 °C temperature range is more responsible than within the 50–400 °C temperature range for the higher TEC. Increasing the A-site cation deficiency suppresses thermal reduction, and within the narrow temperature range of 700–750 °C, a sharp increase in TEC is observed (Fig. 2). No obvious thermal reduction occurs within this temperature range (Fig. 3). Such an abnormal increase
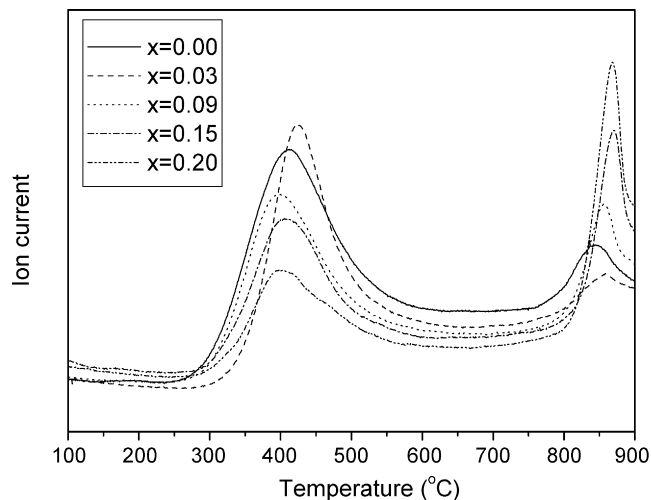

Fig. 2. Linear thermal expansion curves for $(BS)_{1-x}CF$ ($x = 0.00–0.20$) under an air atmosphere.

Fig. 3. O_2–TPD profiles of $(BS)_{1-x}CF$ ($x = 0.00–0.20$) powders.

Table 2
Amount of oxygen desorption for $(BS)_{1-x}CF$ ($x = 0.00$–0.20) oxides, calculated from O_2–TPD

A-site deficiency, x	Oxygen desorbed (mmol g^{-1})		
	α-Oxygen	β-Oxygen	$(\alpha + \beta)$-Oxygen
0.00	1.72	0.233	1.95
0.03	1.55	0.229	1.80
0.09	1.19	0.347	1.53
0.15	0.920	0.503	1.42
0.20	0.680	0.647	1.33

Table 3
Effective ionic radii of cobalt and iron

Element	Ion charge	Effective ionic radii (pm)[a]
	2+	65 LS (low spin)
		74.5 HS (high spin)
Co	3+	54.5 LS
		61 HS
	4+	53 HS
	2+	61 LS
		78 HS
Fe	3+	55 LS
		64.5 HS
	4+	58.5

[a] Coordination number is 6.

in TEC is therefore attributed to the low to high transition of the Co^{2+}/Co^{3+} spin-state, because large variations in ionic size are observed to accompany this spin-state transition (Table 3). These results suggest that A-site cation deficiency successfully suppresses the thermally induced spin-state transition. The abnormal thermal expansion behavior of $(BS)_{0.80}CF$ in the 450–700 °C temperature range may be related to the formation of impurities.

3.3. Electrical conductivity

A cathode material should possess sufficient electrical conductivity to ensure efficient current collection; thus, the effect of A-site cation deficiency on the electrical conductivity of the $(BS)_{1-x}CF$ oxide was investigated, and is presented in Fig. 4. The electrical conductivity of all oxide samples initially increases linearly
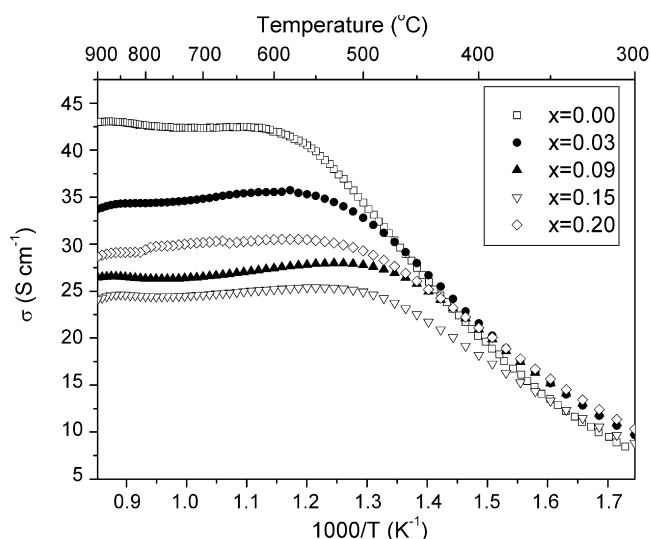
with temperature up to a transition temperature (T_s) between 450 and 550 °C, but after this point the conductivity reaches a plateau for temperatures exceeding T_s (Fig. 4). The thermal reduction of Co^{4+}/Fe^{4+} to Co^{3+}/Fe^{3+} creates additional oxygen vacancies and thus disrupts the O–(Fe,Co)–O periodic potential. This, in turn, decreases the concentration of charge carriers and the covalent interaction, and may cause the observed changes in conductivity [34–36]. Across all values of x examined, the conductivity decreases as the A-site cation deficiency increases. For example, the maximum conductivity of BSCF is 42 S cm^{-1}, but that of $(BS)_{0.8}CF$ is only 25 S cm^{-1}. This trend differs from that observed for A-site cation-deficient $(La_{0.6}Sr_{0.4})_{1-x}Co_{0.2}Fe_{0.8}O_{3-\delta}$ ($x = 0.00$–0.15) perovskite oxides, which show an initial increase in electrical conductivity with increasing A-site cation deficiency for values of x up to 0.05 [24]. Such behavior is closely related to the concurrent transition of the perovskite phase structure from rhombohedral to cubic symmetry. The increased cell symmetry improves overlap between the transition metal 3d orbitals and the oxygen 2p orbitals [24]. Introducing A-site cation deficiency does not, however, improve the cell symmetry of $(BS)_{1-x}CF$, and so the conductivity decreases monotonically from the creation of additional oxygen vacancies. Nevertheless, contrary to expectations, further increases in A-site cation deficiency up to $x = 0.20$ increase conductivity, and this effect may be related to the formation of impurities (Fig. 1).

3.4. Chemical compatibility

The $(BS)_{1-x}CF$ and SDC mixture, which was calcined at 1000 °C for 2 h under an air atmosphere, was analyzed with XRD, and results are presented in Fig. 5. In addition to the characteristic diffraction peaks corresponding to $(BS)_{1-x}CF$ perovskite and SDC fluorite, peaks are also observed at $2\theta = 32.3°$ and $36.3°$. This indicates that a solid-state reaction between $(BS)_{1-x}CF$ and SDC occurred. The impurities, identified as perovskite with the composition $(Ba,Sr,Ce,Sm)(Co,Fe)O_{3-\delta}$, were formed when the Sm^{3+} and Ce^{3+} from the SDC were incorporated into the A-sites of the $(BS)_{1-x}CF$. Wang et al. found that $(Ba,Sr,Ce,Sm)(Co,Fe)O_{3-\delta}$ perovskite oxides have lower catalytic activity for oxygen reduction [37]. Li et al. found that the substitution of the A-site of BSCF by the rare earth elements could reduce the TEC of BSCF slightly [38,39]. Therefore, the formation of impurities may be not detrimental to the long-term stability of the cathode.

Fig. 4. Electrical conductivity of $(BS)_{1-x}CF$ ($x = 0.00$–0.20) oxides under an air atmosphere.
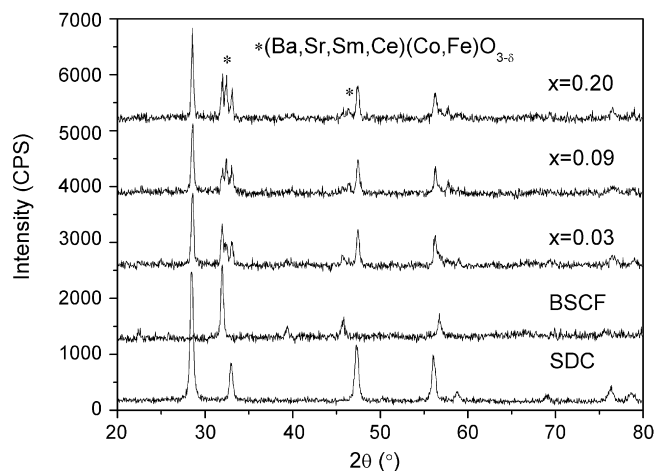
Fig. 5. XRD patterns of SDC, BSCF, and $(BS)_{1-x}CF$ ($x = 0.03$–0.20) + SDC mixtures calcined at 1000 °C for 2 h under an air atmosphere.

3.5. Impedance analysis

The performance of $(BS)_{1-x}CF$ ($x = 0.00$, 0.03, 0.09, and 0.20, fired at 1000 °C) as the cathode in a symmetrical cell configuration was investigated via ac impedance spectroscopy under an air atmosphere. The Nyquist plots of the cells were obtained at 600 °C under open-circuit conditions, and are given in Fig. 6. All impedance spectra contain two separable depressed arcs, suggesting that at least two different electrode processes limit the oxygen reduction reaction. In order to separate these two processes, the impedance spectra were fitted to an equivalent circuit with a standardized configuration (Fig. 6e). The inductances of the circuits, L, may be the result of the Ag current/voltage probes or the high frequency phase shift of the electrochemical equipment. The overall ohmic resistance, R_{ohm}, includes the electrolyte resistance, the electrode ohmic resistance, and the lead resistance. The high-frequency resistance is probably associated with charge-transfer processes (R_{E1}). The low-frequency arc is ascribed to diffusion processes (R_{E2}), including the adsorption–desorption of oxygen, oxygen diffusion at the

gas–cathode interface, and the surface diffusion of intermediate oxygen species [40–47]. Parameters Q_1 and Q_2 are constant phase elements and their impedances are expressed as follows [47]:

$$Q = \frac{1}{B(j\omega)^{\alpha}} \tag{1}$$

where B is a frequency-independent constant, ω is the angular frequency ($\omega = 2\pi f$), j is the square root of -1, and α is an exponential constant. For $\alpha = 1$, 0.5, 0, and -1, Q represents an ideal capacitance, a Warburg impedance, an ideal resistance, and an inductance, respectively.

The fitted impedance parameters are given in Table 4. For the cathode composed of BSCF, which is not cation deficient ($x = 0$), the high-frequency arc is smaller than the low-frequency arc. This implies that surface diffusion processes are the rate-determining step in the oxygen reduction reaction at 600 °C (Fig. 6a). When the A-site cation deficiency increases, the rate-determining step changes from oxygen surface diffusion to charge-transfer processes. It is likely that the additional oxygen vacancies, which are the result
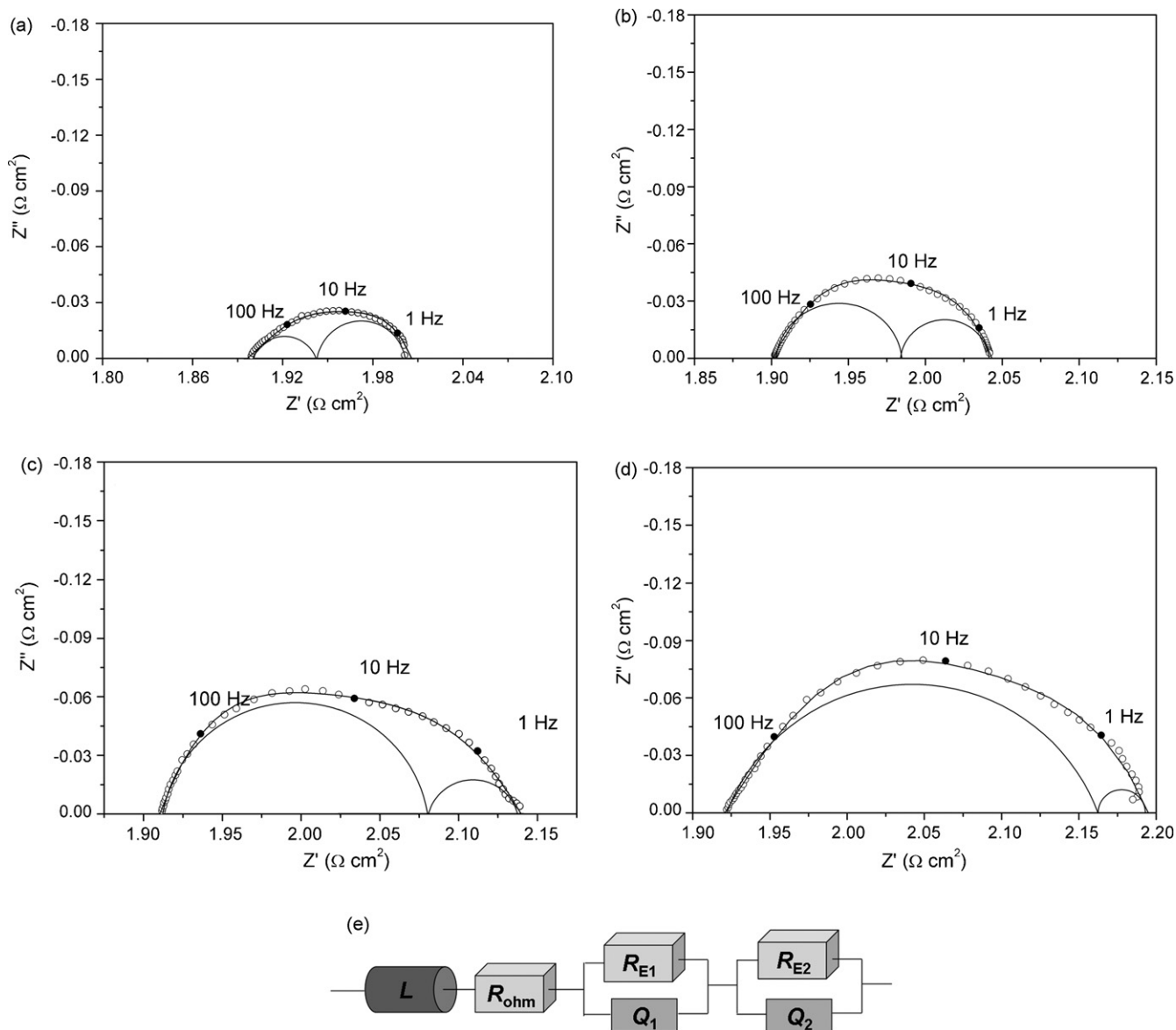

Fig. 6. Nyquist-type impedance curves for $(BS)_{1-x}CF$ (a) $x = 0.00$, (b) $x = 0.03$, (c) $x = 0.09$, and (d) $x = 0.20$. The solid lines are the fitted curves. (e) Equivalent circuit used for fitting the impedance data.

Table 4
Fitted impedance spectra values for $(BS)_{1-x}CF$ ($x = 0.00$–0.20) cathodes at the operating temperature of 600 °C

x	R_{ohm} (Ω cm^2)	R_{E1} (Ω cm^2)	Q_1 ((Fs)$^{1-n}$ cm^{-2})	n_1	R_{E2} (Ω cm^2)	Q_2 ((Fs)$^{1-n}$ cm^{-2})	n_2
0.00	1.899	0.0436	0.1150	0.77	0.0632	0.4325	0.62
0.03	1.902	0.0804	0.1486	0.81	0.0560	1.471	0.86
0.09	1.911	0.1704	0.1120	0.79	0.0491	1.442	0.95
0.20	1.927	0.2388	0.1567	0.75	0.0264	5.652	0.99

of A-site cation deficiency, promote oxygen surface-exchange processes. The reduction in diffusion polarization resistance, however, is smaller than the increase in charge-transfer resistance, and overall cathode performance deteriorates with increased A-site cation deficiency. For example, the diffusion resistance of $(BS)_{0.80}CF$ is reduced by a factor of about 2.5 relative to that of BSCF, but the charge-transfer resistance increases to more than 5.4 times its original value. Consequently, the change in charge-transfer polarization resistance dominates the net change in the polarization resistance of the $(BS)_{0.80}CF$ electrode.

Charge-transfer processes include the ion-transfer processes occurring at electrode/electrolyte interfaces and the electron-transfer processes accompanying oxygen reduction. In order to obtain a better understanding of the relevant charge-transfer processes, the capacitance (C) and relaxation frequency (f) of the simulated circuits were calculated using Eqs. (2) and (3) [48], respectively.

$$C = \frac{(RQ)^{1/n}}{R}, \tag{2}$$

$$f = \frac{\omega}{2\pi}. \tag{3}$$

In Eq. (3), ω is the relaxation frequency, given as follows [49]:

$$\omega = (RQ)^{-1/n} \tag{4}$$

As shown in Table 5, The capacitance and relaxation frequency of the charge-transfer processes occurring with $(BS)_{1-x}CF$ ($x = 0.00$, 0.03, 0.09, and 0.20) are in the ranges of 10–100 mF cm^{-2} and 10–1000 Hz, respectively. Both ranges are typical for the chemical reduction of oxygen accompanied by electron-transfer processes [47,50], while the reported capacitance and relaxation frequency values for the ion-transfer processes of cation-stoichiometric BSCF are 42 μF cm^{-2} and 160 kHz, respectively [51]. In our previous study, we observed that the reciprocal resistance values of the high-frequency arc from BSCF have roughly a 1/4 dependence oxygen partial pressure [52], and this is strong evidence that the electron-transfer steps of oxygen reduction are limited in the BSCF cathode [47]. It also suggested that the high-frequency arc measured in this study can be attributed solely to electron-transfer processes. The increased electron-transfer resistance associated with increased A-site cation deficiency is likely the result of impurities formed at the triple-phase boundary (3PB).
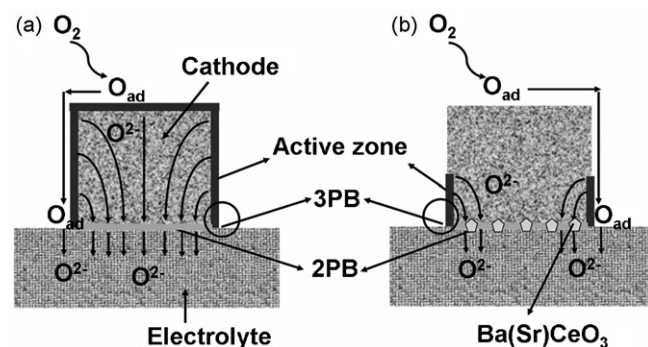
Interestingly, the impurity phases formed at the cathode/electrolyte interface do not have observable effects on ion-transfer processes. This is very different from the case of Ba- and Sr-enriched barium strontium cobalt ferrites, i.e.,

$(Ba_{0.5}Sr_{0.5})_{1.20}Co_{0.8}Fe_{0.2}O_{3-\delta}$ ($(BS)_{1.2}CF$). For these materials, it was found that the solid-state reaction between $BS_{1.2}CF$ and SDC results in the formation of $(Ba,Sr,Ce,Sm)(Co,Fe)O_{3-\delta}$ and $Ba(Sr)CeO_3$ perovskites [53]. Such impurities not only deteriorate electron transfer at the 3PB but also decrease ion transfer at the cathode/electrolyte two-phase boundary (2PB).

This difference in behavior is explained schematically in Fig. 7. Although the $(Ba,Sr,Ce,Sm)(Co,Fe)O_{3-\delta}$ oxides have lower electro-catalytic activity and ionic conductivity than BSCF, their cathodic performances are still superior in IT-SOFCs [37,54]. The BaCeO$_3$ phase, however, has much lower electrocatalytic activity and ionic conductivity than those of $(Ba,Sr,Ce,Sm)(Co,Fe)O_{3-\delta}$ oxides. The formation of BaCeO$_3$ between the $(BS)_{1.20}CF$ and SDC interface significantly inhibits oxide ion transfer across this interface (Fig. 7b). On the other hand, the oxygen ionic conductivity of the cathode material also affects the charge-transfer processes. For the BSCF cathode, which is not cation-deficient, oxygen surface exchange is the rate-determining step in oxygen reduction, because oxygen has a high bulk diffusion rate. This effectively extends the BSCF cathode's active zone of oxygen reduction across the entire cathode surface. Under these conditions, charge transfer occurs at both the gas–cathode–electrolyte 3PB and the gas–cathode two-phase boundary. Since $(BS)_{0.97}CF$ demonstrates higher oxygen permeability than non-cation-deficient BSCF [27], optimizing A-site cation deficiency by setting $x = 0.03$ should enhance the ionic conductivity of the oxide. Although further increasing the A-site cation-deficiency slightly reduces oxygen permeability, the corresponding value is still comparable to that of BSCF [27]. This strongly suggests that the ionic conductivity of $(BS)_{0.80}CF$ is still sufficient to engage the entire cathodic surface in oxygen reduction. The oxygen permeation flux of $(BS)_{1.20}CF$ is 21.8% lower than that of BSCF at 700 °C under the identical operating conditions [55], and this is attributed to the dramatic reduction in ionic conductivity from defect associations. Fleig [56] noted that if oxygen-ion diffusion in the cathode bulk is the rate-determining step, then the active zone is restricted to the 3PB, and the entire ionic current density is concentrated within a distance of only a few nanometers across the 2PB, between the MIEC and the electrolyte (as shown in Fig. 7b). Oxygen reduction on the $(BS)_{1.20}CF$ cathode is likely constricted

Table 5
Capacitance, relaxation frequency and exchange current density of $(BS)_{1-x}CF$ ($x = 0.00$–0.20) at the operating temperature of 600 °C

	x			
	0.00	0.03	0.09	0.20
C_1 (mF cm^{-2})	23.6	52.6	39.1	52.4
f_1 (Hz)	154.3	37.60	23.90	12.70
I_0 (mA cm^{-2})	431.4	234.0	110.4	78.77

Fig. 7. Schematic of the oxygen reduction mechanism with (a) $BS_{0.80}CF$ or (b) $BS_{1.20}CF$ cathodes.
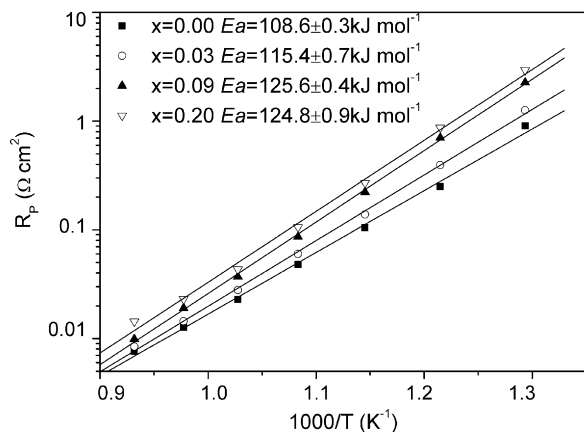
Fig. 8. Temperature dependence of R_p for $(BS)_{1-x}CF$ ($x = 0.00–0.20$) cathodes.

to the 3PB, and this increases the polarization resistance for the ion-transfer processes.

Finally, the exchange current density, I_0, which is a direct reflection of the electrocatalytic activity, is calculated from the charge-transfer resistance (R_{E1}) according to the Bulter–Volmer equation as follows [57]:

$$I_0 = \frac{RT}{nFR_{E1}} \tag{5}$$

where n is the number of electrons that contribute to charge transfer reaction, R is the gas constant ($8.3145\,J\,mol^{-1}\,K^{-1}$), F is the Faraday constant ($96485.3\,C\,mol^{-1}$), and T is the absolute temperature (K). For oxygen reduction, n is assumed to be 4. The value of I_0 for $(BS)_{0.80}CF$ at $600\,°C$ is $78.7(7)\,mA\,cm^{-2}$, which is only about 18.2% of that for BSCF (Table 5). These results indicate that impurities between the cathode and the electrolyte interface diminish the electrocatalytic activity and the electrical conductivity of A-site cation-deficient $(BS)_{1-x}CF$. The temperature dependence of the cathode polarization resistances (R_p) for $(BS)_{1-x}CF$ is shown in Fig. 8. As expected, increasing the A-site cation deficiency increases both the area specific resistances (ASR) and the activation energies (E_a) of the cathode.

3.6. Fuel cell performance

The $(BS)_{0.97}CF$ material displays the most promise for application in SOFCs, because it demonstrated high electrocatalytic oxygen reduction activity and low TEC relative to BSCF. We built whole SOFCs constructed with BSCF and $(BS)_{0.97}CF$ cathodes and thin-film SDC electrolyte. The performances of these cells were then measured in terms of their respective power and current densities using humidified H_2 ($3\,mol\%\,H_2O$) as the fuel and ambient air as the oxidant at temperatures between 550 and $650\,°C$; these results are presented in Fig. 9. The cell equipped with the $(BS)_{0.97}CF$ cathode achieves peak power densities of 694 and $893\,mW\,cm^{-2}$ at 600 and $650\,°C$, respectively. These values are slightly lower than those of the cell equipped with the BSCF cathode (728 and $989\,mW\,cm^{-2}$ at 600 and $650\,°C$, respectively). The total electrode polarization resistance, which is the sum of the anode and cathode values, was measured under OCV conditions. The electrode area-specific resistance is only $0.138\,\Omega\,cm^2$ at $600\,°C$ in the cell equipped with the $(BS)_{0.97}CF$ cathode, which is lower than the target value of $0.15\,\Omega\,cm^2$ proposed by Steele for solid-oxide fuel cells operating at reduced temperatures [58]. Unfortunately, the value is still somewhat higher than that of the cell equipped with the BSCF cathode ($\sim0.091\,\Omega\,cm^2$). Nevertheless, the introduction of A-site cation
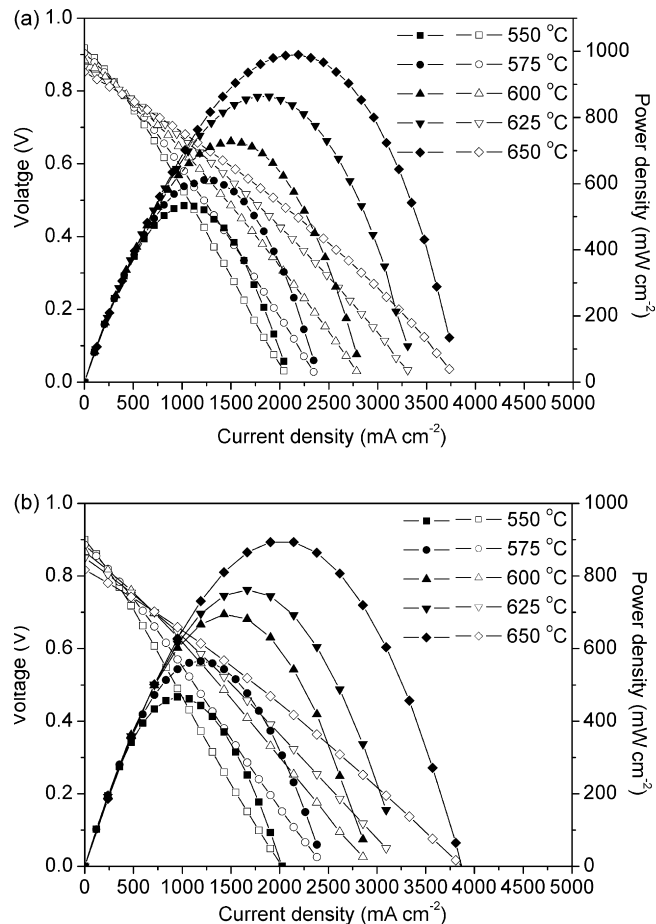

Fig. 9. I–V and I–W curves for SOFCs with (a) $BS_{1.00}CF$ and (b) $BS_{0.80}CF$ cathodes.

deficiency dramatically minimizes the TEC, and this is beneficial for the long-term stability of the fuel cell. The optimized A-site cation-deficient material, $(BS)_{0.97}CF$, is a promising new cathode material for application in intermediate-temperature SOFCs.

4. Conclusions

The extent of A-site cation deficiency has significant effects on both the physical-chemical properties and the electrochemical characteristics of $(BS)_{1-x}CF$ oxides. Pure-phase perovskite with cubic symmetry is obtained for stoichiometric coefficients (x) of values less than 0.15. Increasing A-site cation deficiency decreases electrical conductivity due to the creation of additional oxygen vacancies. The increasing the A-site cation deficiency also causes impurities to form at the cathode/electrolyte interface, and these impurities steadily increase the cathode polarization resistance. The most significant advantage afforded by introducing A-site cation deficiency, however, is the reduction in the thermal expansion coefficient of the material. This effect presumably results from the temperature-induced reduction of the material's cobalt and iron ions from their +4 to their +3 oxidation states and from the suppression of cobalt ion spin-state transitions. The reduction in TEC renders the oxide more compatible with the electrolyte layer, and this is presumably beneficial for long-term stability of any fuel cells incorporating these materials. The SOFC constructed with a $BS_{0.97}CF$ cathode generates peak power densities of 694 and $893\,mW\,cm^{-2}$ at 600 and $650\,°C$, respectively. These values are comparable to those obtained with a $Ba_{0.5}Sr_{0.5}Co_{0.8}Fe_{0.2}O_{3-\delta}$ cathode. In conclusion, slightly A-site cation-deficient $(BS)_{1-x}CF$ is a

promising cathode material for application in reduced temperature SOFCs.

Acknowledgements

References

[1] T. Kenjo, M. Nishiya, Solid State Ionics 57 (1992) 295–302.
[2] M.J.L. Ostergard, C. Clausen, C. Bagger, M. Mogensen, Electrochim. Acta 40 (1994) 1971–1981.
[3] D. Hirabayashi, A. Tomita, S. Teranishi, T. Hibino, M. Sano, Solid State Ionics 176 (2005) 881–887.
[4] T. Hibino, A. Hashimoto, T. Inoue, J. Tokuno, S. Yoshida, M. Sano, Science 288 (2000) 2031–2033.
[5] E.P. Murray, S.A. Barnett, Solid State Ionics 143 (2001) 265–273.
[6] C. Xia, L. Yang, G. Meng, Fuel Cells 4 (2004) 41–47.
[7] M. Juhl, S. Primdahl, C. Manon, M. Mogensen, J. Power Sources 61 (1996) 173–181.
[8] W. Zhou, Z.P. Shao, R. Ran, H.X. Gu, W.Q. Jin, N.P. Xu, J. Am. Ceram. Soc. 91 (2008) 1155–1162.
[9] E. Perry Murray, M.J. Sever, S.A. Barnett, Solid State Ionics 148 (2002) 27–34.
[10] B.C.H. Steele, J.-M. Bae, Solid State Ionics 106 (1998) 255–261.
[11] W.G. Wang, M. Mogensen, Solid State Ionics 176 (2005) 457–462.
[12] H. Fukunaga, M. Koyama, N. Takahashi, C. Wen, K. Yamada, Solid State Ionics 132 (2000) 279–285.
[13] C. Xia, W. Rauch, F. Chen, M. Liu, Solid State Ionics 149 (2002) 11–19.
[14] T. Ishihara, M. Honda, T. Shibayama, H. Minami, H. Nishiguchi, Y. Takita, J. Electrochem. Soc. 145 (1998) 3177–3183.
[15] S.Z. Wang, Y.M. Zou, Electrochem. Commun. 8 (2006) 927–931.
[16] Z.H. Chen, R. Ran, W. Zhou, Z.P. Shao, S.M. Liu, Electrochim. Acta 52 (2007) 7343–7351.
[17] J. Peña-Martínez, D. Marrero-López, J.C. Ruiz-Morales, B.E. Buergler, P. Núñez, L.J. Gauckler, Solid State Ionics 177 (2006) 2143–2147.
[18] W. Zhou, Z.P. Shao, R. Ran, Z.H. Chen, P.Y. Zeng, H.X. Gu, W.Q. Jin, N.P. Xu, Electrochim. Acta 52 (2007) 6297–6303.
[19] W. Zhou, Z.P. Shao, R. Ran, P.Y. Zeng, H.X. Gu, W.Q. Jin, N.P. Xu, J. Power Sources 168 (2007) 330–337.
[20] W. Zhou, R. Ran, Z.P. Shao, H.X. Gu, W.Q. Jin, N.P. Xu, J. Power Sources 174 (2007) 237–245.
[21] Z.P. Shao, S.M. Haile, Nature 431 (2004) 170–173.
[22] G.Ch. Kostogloudis, Ch. Ftikos, Solid State Ionics 126 (1999) 143–151.
[23] A. Mineshige, J. Izutsu, M. Nakamura, K. Nigaki, J. Abe, M. Kobune, S. Fujii, T. Yazawa, Solid State Ionics 176 (2005) 1145–1149.
[24] K.K. Hansen, K. Vels Hansen, Solid State Ionics 178 (2007) 1379–1384.
[25] R. Doshi, V.L. Richard, J.D. Carter, X.P. Wang, M. Krumpelt, J. Electrochem. Soc. 146 (1999) 1273–1278.
[26] L. Bedel, A.-C. Roger, J.-L. Rehspringer, Y. Zimmerman, A. Kiennemann, J. Catal. 235 (2005) 279–294.
[27] L. Ge, W. Zhou, R. Ran, S.M. Liu, Z.P. Shao, W.Q. Jin, N.P. Xu, J. Membr. Sci. 306 (2007) 318–328.
[28] W. Zhou, Z.P. Shao, W.Q. Jin, J. Alloys Compds. 426 (2006) 368–374.
[29] Z.P. Shao, W.S. Yang, Y. Cong, H. Dong, J.H. Tong, G.X. Xiong, J. Membr. Sci. 172 (2000) 177–188.
[30] C.R. Xia, M.L. Liu, J. Am. Ceram. Soc. 84 (8) (2001) 1903–1905.
[31] D. Kek, P. Panjan, E. Wanzenberg, J. Eur. Ceram. Soc. 21 (2001) 1861–1865.
[32] M. Mori, N.M. Sammes, Solid State Ionics 146 (2000) 301–312.
[33] M.A. Peña, J.L.G. Fierro, Chem. Rev. 101 (2001) 1981–2018.
[34] K.T. Lee, A. Manthiram, J. Power Sources 158 (2006) 1202–1208.
[35] K.T. Lee, A. Manthiram, Chem. Mater. 18 (2006) 1621–1626.
[36] H. Takahashi, F. Munakata, M. Yamanaka, Phys. Rev. B 57 (1998) 15211–15218.
[37] K. Wang, R. Ran, W. Zhou, H. Gu, Z.P. Shao, J. Ahn, J. Power Sources 179 (2008) 60–68.
[38] S.Y. Li, Z. Lü, B. Wei, X.Q. Huang, J.P. Miao, G. Cao, R.B. Zhu, W.H. Su, J. Alloys Compd. 426 (2006) 408–414.
[39] S.Y. Li, Z. Lü, X.Q. Huang, W.H. Su, Solid State Ionics 178 (2008) 1853–1858.
[40] S.B. Adler, J.A. Lane, B.C.H. Steele, J. Electrochem. Soc. 143 (1996) 3554–3564.
[41] X.J. Chen, S.H. Chan, K.A. Khor, Electrochim. Acta 49 (2004) 1851–1861.
[42] F. Qiang, K.N. Sun, N.Q. Zhang, X.D. Zhu, S.R. Le, D.R. Zhou, J. Power Sources 168 (2007) 338–345.
[43] S.B. Adler, Solid State Ionics 111 (1998) 125–134.
[44] M.J. Jørgensen, M. Mogensen, J. Electrochem. Soc. 148 (2001) A433–A442.
[45] S.P. Jiang, W. Wang, J. Electrochem. Soc. 152 (2005) A1398–A1408.
[46] M. Koyama, C. Wen, T. Masuyama, J. Otomo, H. Fukunaga, K. Yamada, K. Eguchi, H. Takahashi, J. Electrochem. Soc. 148 (2001) A795–A801.
[47] M.J. Escudero, A. Aguadero, J.A. Alonso, L. Daza, J. Electroanal. Chem. 611 (2007) 107–116.
[48] A. Bierberle-Hütter, M. Sogaard, H.L. Tuller, Solid State Ionics 177 (2006) 1969–1975.
[49] D. Marrero-López, J. Canales-Vázquez, J.C. Ruiz-Morales, A. Rodríguez, J.T.S. Irvine, P. Núñez, Solid State Ionics 176 (2005) 1807–1816.
[50] R. Barfod, M. Mogensen, T. Klemensø, A. Hagen, Y.-L. Liu, P.V. Hendriksen, J. Electrochem. Soc. 154 (2007) B371–B378.
[51] F.S. Baumann, J. Fleig, H.-U. Habermeier, J. Maier, Solid State Ionics 177 (2006) 3187–3191.
[52] W. Zhou, R. Ran, Z.P. Shao, R. Cai, W.Q. Jin, N.P. Xu, J. Ahn, Electrochim. Acta 53 (2008) 4370–4380.
[53] W. Zhou, R. Ran, Z.P. Shao, W. Zhuang, J. Jia, H.X. Gu, W.Q. Jin, N.P. Xu, Acta Mater., doi:10.1016/j.actamat.2008.02.002.
[54] S.Y. Li, Z. Lü, N. Ai, K.F. Chen, W.H. Su, J. Power Sources 165 (2007) 97–101.
[55] L. Ge, R. Ran, K. Zhang, S.M. Liu, Z.P. Shao, J. Membr. Sci., doi:10.1016/j.memsci.2008.02.015.
[56] J. Fleig, J. Power Sources 105 (2002) 228–238.
[57] Y. Matsuzaki, I. Yasuda, Solid State Ionics 126 (1999) 307–313.
[58] B.C.H. Steele, A. Heinzel, Nature 414 (2001) 345–352.